Korean J. Chem. Eng., 32(7), 1314-1322 (2015)
DOI: 10.1007/s11814-014-0339-1

pISSN: 0256-1115
eISSN: 1975-7220

Adsorptive removal of Cr(VI) from aqueous solutions by cross-linked chitosan/bentonite composite

Qian Liu*, Bingchao Yang, Lujie Zhang*, and Ruihua Huang*,†**

*College of Science, Northwest A&F University, Yangling, Shaanxi 712100, China
**Xi'an Institute of Geology and Mineral Resource, Xi'an, Shaanxi 710054, China
(*Received 1 April 2014 • accepted 17 November 2014*)

Abstract−Cross-linked chitosan/bentonite composite (CCB) was prepared, and characterized by Fourier transform infrared (FTIR) spectroscopy, BET surface area and pore diameter analyses, X-ray diffraction (XRD) patterns and thermal gravimetric analyses (TGA). The adsorption of hexavalent chromium Cr(VI) onto CCB as a function of adsorbent dosage, initial Cr(VI) concentration, solution pH, and contact time was investigated through batch experiments. The removal towards Cr(VI) decreased with increasing solution pH from 2 to 11 and initial Cr(VI) concentration, while it increased with increasing adsorbent dosage. The adsorption kinetic data of Cr(VI) on CCB were well described by the pseudo-second-order model. The equilibrium data were correlated by the Langmuir isotherm model. The maximum monolayer Cr(VI) adsorption capacity for CCB at pH 2 and 293 K was 89.13 mg/g. The mechanisms for the adsorption of Cr(VI) on CCB at pH 2 may include electrostatic interaction and chemical interaction between CCB and Cr(VI) ions.

Keywords: Cross-linked Chitosan/Bentonite Composite, Adsorption, Cr(VI), Kinetics, Isotherm

INTRODUCTION

Chromium is a common pollutant introduced via the discharge of a variety of industrial wastewaters like electroplating, leather tanning, wood preservations, manufacturing of dye, paint and paper [1]. Chromium exists in the environment as trivalent [Cr(III)] and hexavalent [(Cr)] forms and Cr(VI) is considered highly toxic, carcinogenic and mutagenic. Therefore, it is very essential to control the concentration of Cr(VI) in wastewater before its disposal into the environment. To remove hexavalent chromium Cr(VI) during water treatment, a great variety of processes have been developed, such as chemical precipitation, electrochemical precipitation, ion exchange, solvent extraction and adsorption. But these methods are expensive and ineffective especially when the heavy metal ions are present in the wastewater at low concentrations. Adsorption has been considered effective for the removal of toxic metals from aqueous environment due to its simplicity of design, ease of operation and high efficiency [2-4].

Recently, there has been a great interest in development of new adsorbents for effective removal of Cr(VI) from aqueous solutions [5,6]. Chitosan has received much attention as an excellent natural adsorbent to remove many pollutants including fluoride, dyes, and heavy metal ions due to the presence of amino and hydroxyl groups, which can serve as the active sites [7-9]. However, raw chitosan agglomerates and forms a gel in aqueous medium, so most of the hydroxyl and amino groups are inaccessible for metal binding. In addition, raw chitosan is very sensitive to pH due to its dissolution in acidic media [10,11]. To improve its adsorption capacity and resistance to acidic environment, the design and exploration of novel adsorbents based on chitosan are still necessary. The synthesis of biocomposites has presented a novel approach. At present, different kinds of substances have been used to form composites with chitosan such as sand, bentonite [12,13], montmorillonite [14, 15], and hydroxyapatite [16], etc.

Bentonite, having larger surface area than silica or zeolite, is a kind of expandable clay mineral consisting primarily of montmorillonite. It can be easily modified by intercalating inorganic/organic cations, and the resulting products are more efficient adsorbents than the original one due to the increased surface area and more functional groups. Therefore, with an objective to improve its resistance in acidic medium, to make the binding sites readily available for the adsorbate and to increase the adsorption capacity of bentonite or chitosan, we applied a combination of physical and chemical modification, where chitosan would intercalate in bentonite and be cross-linked with glutaraldehyde (GLA), and prepared a composite chitosan biosorbent. In this study, the cross-linked chitosan/bentonite composite (CCB) was characterized by Fourier transform infrared (FTIR) spectroscopy and X-ray diffraction (XRD) patterns. The removal towards Cr(VI) ions from aqueous solutions by CCB was evaluated. Experimental parameters affecting the adsorption process such as solution pH, initial Cr(VI) ions concentration, adsorbent dosage and contact time were studied. The experimental adsorption data were also analyzed by different kinetic and isotherm models.

MATERIALS AND METHODS

1. Materials

Chitosan was purchased from the Sinopharm Group Chemical

†To whom correspondence should be addressed.
E-mail: huangrh20022002@aliyun.com

Reagent Limited Company (China). Bentonite powder with a particle size of 200-mesh was acquired from the chemical factory of Shentai, Xinyang, Henan, China. All other chemicals used were of analytical grade (e.g., acetic acid, sodium hydroxide, potassium dichromate). The stock solution of Cr(VI) was prepared by dissolving potassium dichromate in de-ionized water. The desired pH was adjusted by adding 0.1 mol/L HCl or 0.1 mol/L NaOH solutions.

2. Preparation of Cross-linked Chitosan/Bentonite Composite (CCB)

The CCB was prepared as follows. Chitosan solution was prepared by dissolving 2 g of chitosan in 100 mL of 2 wt% acetic acid solution with continuous stirring. 2 g of natural bentonite was then added to the chitosan solution, and the reaction system was continued to be stirred for 2 h at room temperature. After that, 25 wt% glutaraldehyde (GLA) solution was added into the above solution and the ratio of glutaraldehyde to chitosan was approximately 5 mL/g of chitosan. Cross-linking reaction occurred for 23 h at 60 °C and the resulting CCB was allowed to settle, washed with de-ionized water to remove any free GLA and dried at 60 °C. Finally, the dried CCB was ground and sieved to obtain a particle size of 200-mesh for adsorption experiments.

3. Instrumentation

We used X-ray diffraction (XRD) patterns to characterize the structures of natural chitosan, bentonite, chitosan/bentonite composite and cross-linked chitosan/bentonite composite using a Shimadzu XD3A diffractometer equipped with a monochromatic Cu Ka source (λ=0.154 nm) operating at 40 kV and 30 mA. The diffraction patterns were recorded from 3° to 55° with a scan rate of 0.02°/s. The specific surface area analysis of chitosan, bentonite, chitosan/bentonite composite, and CCB was performed using BET method after N_2 adsorption-desorption at 77 K with V-Sorb 2800P surface area and pore distribution analyzer. The change in the structure of CCB before and after Cr(VI) adsorption was determined by FTIR. Spectra were collected with a spectrometer using KBr pellets. In each case, 1 mg of dried samples and 100 mg of KBr were homogenized using mortar and pestle, thereafter pressed into a transparent tablet. The pellets were analyzed with an FTIR Spectrometer (Shimadzu 4100) in the transmittance (%) mode with a scan resolution of 4 cm^{-1} in the range 4,000-400 cm^{-1}. Thermal gravimetric analyses (TGA) were performed on natural chitosan and cross-linked chitosan/bentonite composite samples using Perkin-Elmer Diamond TA/TGA in the temperature range of 27-800 °C at a heating rate of 10 °C per minute.

4. Batch Adsorption Experiments

To study the effect of various parameters (pH, adsorbent dosage, initial concentration and contact time), batch experiments were conducted at 293 K. The solution pH was adjusted to a given value by adding either 0.1 mol/L HCl or 0.1 mol/L NaOH solutions before adsorption experiment. Adsorption experiments were conducted in conical flasks containing 50 mL of Cr(VI) solution prepared from the dilution of 1 g/L stock solutions. At the end of predetermined time intervals, the adsorbate was filtered and Cr(VI) concentration was determined. All experiments were done twice and the adsorbed concentrations given were the means of duplicated experimental results. The experimental error was below 4%, and the average data were reported. The removal towards Cr(VI) was calculated as follows:

$$\%\text{Removal} = \frac{C_0 - C_t}{C_0} \times 100\% \quad (1)$$

where C_0 is the initial concentration (mg/L) and C_t is the final concentration (mg/L). The value for q_t is the amount of Cr(VI) adsorbed per specific amount of adsorbent (mg/g) at any time, t. The adsorption capacity at time t, q_t (mg/g) was obtained as follows:

$$q_t = \frac{(C_0 - C_t)V}{m} \quad (2)$$

where V was the solution volume and m is the mass of CCB.

RESULTS AND DISCUSSION

1. Characterization of Cross-linked Chitosan/Bentonite Composite

Fig. 1 shows the XRD patterns of natural chitosan, bentonite, chitosan/bentonite composite and cross-linked chitosan/bentonite composite. For chitosan/bentonite composite, its preparation was similar to that of cross-linked chitosan/bentonite composite. What was different was that the mixed solution was adjusted to neutral with 0.1 mol/L NaOH solution after the reaction between chitosan and bentonite occurred for 23 h without GLA cross-linking. The XRD pattern of chitosan (Fig. 1(a)) has low crystallinity and the characteristic peaks at 2θ=11.2° and 22.4° are assigned to semi-crystalline structures [17]. The XRD pattern for bentonite (Fig. 1(b)) exhibited a typical reflection peak of montmorillonite at 2θ=6.56°, corresponding to a d_{001} spacing of 1.346 nm. After chitosan interacted with bentonite and chitosan was cross-linked with GLA, the

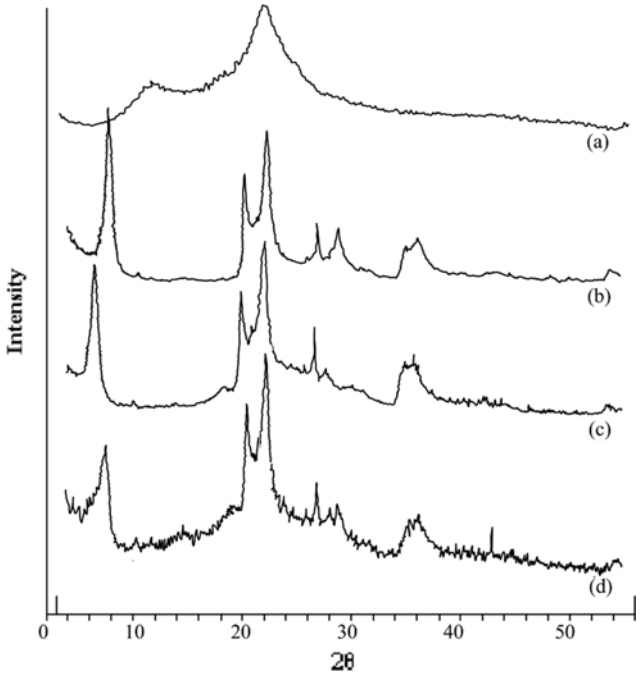

Fig. 1. XRD patterns of chitosan (a), bentonite (b), cross-linked chitosan/bentonite composite (c) and chitosan/bentonite composite (d).

Table 1. Physical properties of chitosan, bentonite, chitosan/bentonite composite and CCB

	Chitosan	Bentonite	Chitosan/bentonite composite	CCB
Total pore volume (cm^3/g)	0.0142	0.0863	0.0608	0.0462
Average pore diameter (nm)	10.505	7.743	15.205	15.993
Micropore area (m^2/g)	0.205	28.132	15.397	11.084
BET surface area (m^2/g)	3.983	37.678	15.984	11.548
Langmuir surface area (m^2/g)	5.096	45.345	21.968	15.662

diffraction peaks, which are typical fingerprints of semi-crystalline chitosan, disappeared, indicating that the crystallinity degree of chitosan was destroyed. Furthermore, the d_{001} spacing of montmorillonite in cross-linked chitosan/bentonite composite (Fig. 1(c)) was slightly increased to 1.457 nm (2θ=6.06°), indicating the intercalation of chitosan into the bentonite interlayer region. However, chitosan/bentonite composite (Fig. 1(d)) had no changes in the peak's position at 2θ=6.56°, indicating that chitosan did not intercalate in bentonite.

Table 1 presents changes of the surface area, average pore size and other physical properties of chitosan, bentonite, chitosan/bentonite composite and CCB. According to Table 1, chitosan is observed to have the least specific surface area while bentonite has the highest surface area. Chitosan/bentonite composite resulted in a larger surface area than that of chitosan but less than that of bentonite. Further reduction in the surface area was observed for CCB. The specific surface area, micropore area and total pore volume are in the order of bentonite>chitosan/bentonite composite>CCB>chitosan. Chitosan/bentonite composite and CCB have "inferior" properties in comparison to bentonite, owing to formation of a flocculated structure, where an intermolecular hydrogen bond was formed between the hydroxylated edge-edge silicate layers and the amino (-NH_2) or hydroxyl (-OH) functional group of chitosan [18]. The lower surface areas of chitosan/bentonite composite and CCB were attributed to the compact packing of chitosan molecules in the surface of bentonite or the interlayer space of bentonite, resulting in pore blocking that inhibited the passage of nitrogen molecules [19].

FTIR spectrum is a useful tool to identify functional groups in molecules, and can obtain structural and bond information on a complex. FTIR spectrum of this composite is shown in Fig. 2(a). The major bands for chitosan can be assigned as follows: 3,444 cm^{-1} (-OH and -NH_2 stretching vibrations), 2,929 cm^{-1} (-CH stretching vibration in -CH and -CH_2), 1,652 cm^{-1} (N-H bending vibration), 1,405 cm^{-1} (-CH symmetric bending vibrations in -CHOH-), 1,084 and 1,039 cm^{-1} (-CO stretching vibration in -COH), and another peak was observed at 1,566 cm^{-1} attributed to the bending vibrations of amine (-NH_2) group [20,21]. Besides, the bands corresponding to the bentonite structure occur between 470 and 1,120 cm^{-1} and are associated with the stretching and angular deformations of the Si-O-Si and Si-O-Al bonds [22]. The characteristic stretching band of the Si-O bond appears between 1,040 and 1,100 cm^{-1} [23], and the angular deformation of Si-O is in the 523-525 cm^{-1} range. The bands from 920 to 800 cm^{-1} correspond to the octahedral layers. Fig. 2(b) represents the FTIR spectrum of this composite adsorbed Cr(VI), which is almost similar to the one of CCB except the peak at 1,566 cm^{-1}. It was not difficult to find that the peak at 1,566 cm^{-1} attributed to the bending vibrations of amine group almost disappeared after Cr(VI) adsorption. This peak at 1,652 cm^{-1} clearly weakened, suggesting the involvement of amine groups in the adsorption of Cr(IV) ions onto CCB. This phenomenon also explains the possible ionic attraction between -NH_3^+ groups in CCB and $Cr_2O_7^{2-}$ groups.

Thermal stability of the composites was evaluated by thermogravimetric analysis, and results are shown in Fig. 3. The two samples exhibited three stages of weight loss. In the first stage, slight

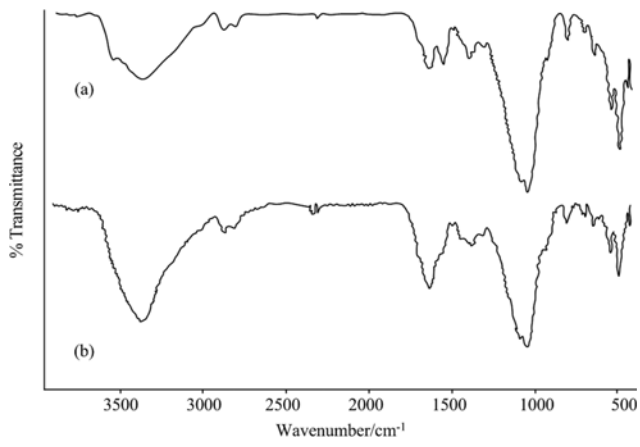

Fig. 2. FTIR spectra of cross-linked chitosan/bentonite composite before adsorption (a) and after adsorption (b).

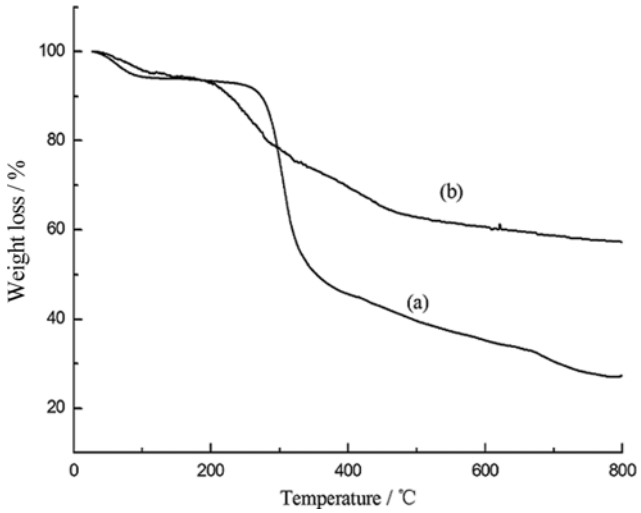

Fig. 3. TG plots of chitosan (a) and CCS/BT composite (b).

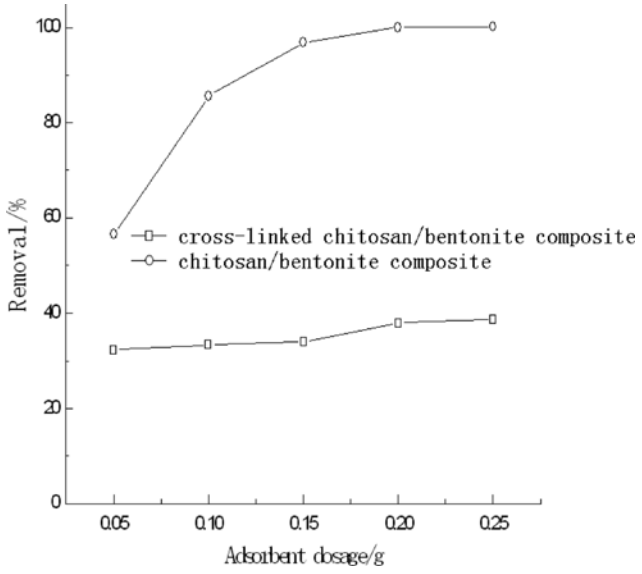

Fig. 4. Effect of CCB dosage on Cr(VI) adsorption.

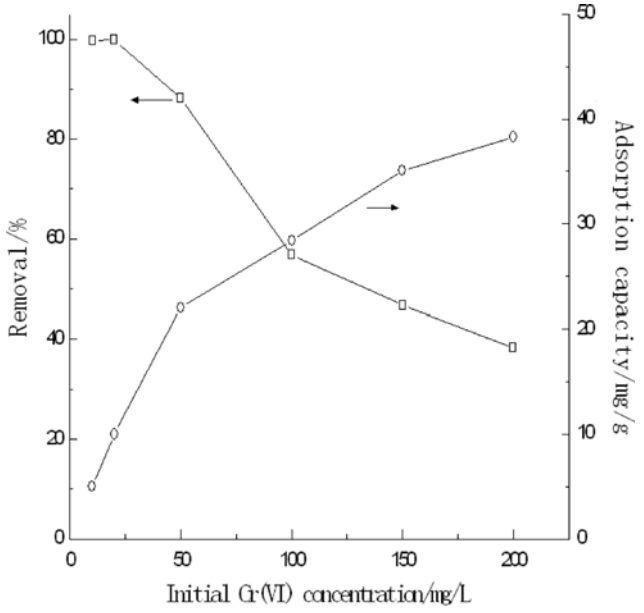

Fig. 5. Effect of initial Cr(VI) concentration on Cr(VI) adsorption.

weight loss was presented at <200 °C. In the second stage, major weight loss is observed from 280 °C to 330 °C and 200 °C to 480 °C for chitosan and CCB composite, respectively. The main weight loss for chitosan and CCB composite was 50% and 30%, respectively. Subsequently, a slow weight loss was observed. The weight loss of chitosan is higher than that of CCB composite at high temperatures. Thus, the thermal stability of the CCB composite is improved because of the addition of clay particles (bentonite) to cross-linked chitosan.

2. Effect of CCB Dosage on Cr(VI) Adsorption

The effect of CCB dosage was studied at the dosage between 0.05 g and 0.25 g in 50 mL aqueous solution. These tests were conducted at 293 K and natural pH value. The initial Cr(VI) ion concentration was 50 mg/L. The removal towards Cr(VI) onto CCB increased rapidly with the increasing of adsorbent concentration (Fig. 4). This result was expected because an increase in adsorbent dosage leads to greater sites available for Cr(VI) adsorption. When the adsorbent concentration was increased from 0.05 to 0.15 g, the removal towards Cr(VI) ions increased from 56.5 to 96.8%. At higher concentrations, the removal towards Cr(VI) did not increase significantly with increasing CCB dosage. For subsequent studies, 0.1 g CCB was selected because CCB at this dosage presented a moderate removal (>85%) towards Cr(VI). Besides, it was not difficult to find that cross-linked chitosan/bentonite composite showed obviously higher removals towards Cr(VI) than chitosan/bentonite composite. This trend may be explained like that. Though cross-linking was at the cost of the loss of active groups such as hydroxyl and amino groups, and reduced the binding sites for Cr(VI), chitosan intercalated in bentonite during the cross-linking process, and an increase in interlayer spacing was observed. The bigger interlayer spacing facilitated the adsorption of Cr(VI) onto CCB, leading to an increase in removal.

3. Effect of Initial Cr(VI) Concentration on Cr(VI) Adsorption

Cr(VI) ions solutions with different concentrations from 10 to 200 mg/L were used; the experiments were carried out at 293 K and natural pH value with contact time of 150 min. From the experimental studies, the removal towards Cr(VI) decreased from 99.8 to 38.3% with increasing initial Cr(VI) concentration (Fig. 5). At low initial concentrations, the Cr(VI) removal was higher due to a larger surface area of CCB being available for the adsorption of Cr(VI) ions. When the Cr(VI) concentration became higher, the removal was lower because the available sites of adsorption became less. At a higher initial concentration, the ratio of initial number of Cr(VI) to the available adsorption surface area was higher, fewer sites were used for adsorption, and as a result the removal decreased. As the initial Cr(VI) concentration increased from 10 to 200 mg/L, the

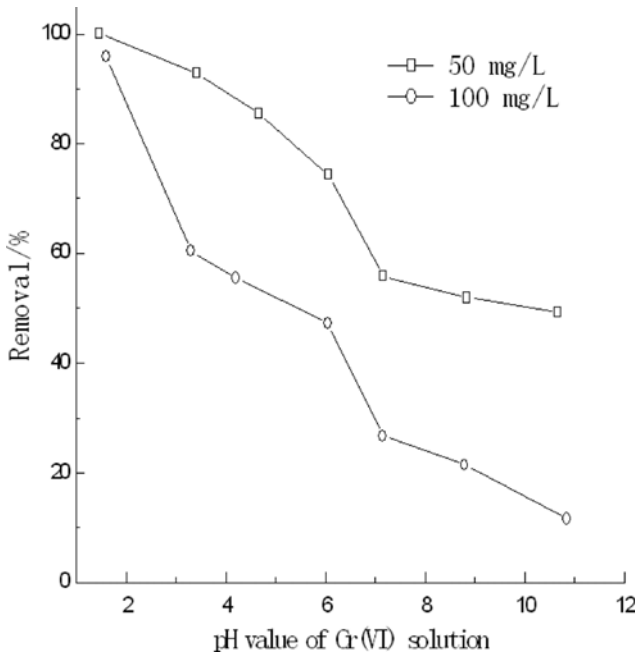

Fig. 6. Effect of solution pH on Cr(VI) adsorption.

adsorption capacity of Cr(VI) onto CCB increased from 4.98 to 38.3 mg/g. This indicates that the initial Cr(VI) concentration played an important role in the adsorption capacity. With increasing Cr(VI) concentration, more Cr(VI) would be in the vicinity of CCB active sites, hence the absolute amount removed of Cr(VI) would increase.

4. Effect of Solution pH on Cr(VI) Adsorption

The effect of solution pH on Cr(VI) adsorption by CCB was investigated in the pH range 2-11 with the Cr(VI) concentrations of 50 mg/L and 100 mg/L. Fig. 6 shows that the removal towards Cr(VI) decreased obviously with an increase in pH values of Cr(VI) solutions from 2 to 11. This indicates that the adsorption of Cr(VI) on CCB was favored at lower pH value. As we know, the existing form of Cr(VI) is greatly dependent upon the pH and concentration of the solution. At pH value below 1, the predominant species is H_2CrO_4 (chromic acid). In acidic media around 2, Cr(VI) exists mostly in the form of dichromate ($Cr_2O_7^{2-}$) ions. At pH between 2 and 6, $Cr_2O_7^{2-}$ and chromate (CrO_4^{2-}) exist in equilibrium and under alkaline conditions (pH>8), it exists predominantly as $HCrO_4^-$ [24]. The pH dependence of Cr(VI) adsorption can largely be related to type and ionic state of these functional groups in adsorbent and also on the Cr(VI) chemistry in solution [25]. Though the pH value of Cr(VI) changed, Cr(VI) ions normally exist in the anionic form. However, at lower pH, parts of -NH_2 groups were protonated; therefore, increasing electrostatic attraction between negatively charged Cr(VI) ions and positively charged adsorption sites resulted in an increase in the adsorption of Cr(VI) ions onto CCB. With increasing pH, the amine groups of chitosan were deprotonated and abundant OH^- ions created a competitive environment with anionic Cr(VI) ions for the adsorption sites; thus the removal decreased.

5. Effect of Contact Time on Cr(VI) Adsorption

The effect of contact time on Cr(VI) ions by CCB was tested with the Cr(IV) concentration of 100, 200 and 300 mg/L at 293 K and pH 2. Fig. 7 shows that the rate of Cr(IV) adsorption was rapid initially and then slowed down gradually until equilibrium was reached, beyond which there was no further adsorption. This was because a large number of vacant surface sites were available for adsorption during the initial stage, and after a lapse of time, the remaining vacant surface sites were difficult to occupy due to repulsive forces between the adsorbate molecules in the aqueous solution and those on the adsorbent surface [26]. Similar results have been reported by Gupta and Babu for the Cr(IV) adsorption on sawdust [27]. Besides, longer equilibrium time was required with increasing initial Cr(IV) concentrations, and the time needed for Cr(IV) ions at 100, 200, and 300 mg/L to reach equilibrium was 80, 120, and 150 min, respectively. For the sake of the attainment of equilibrium, an equilibrium time of 240 min was considered to be optimum in further experiments.

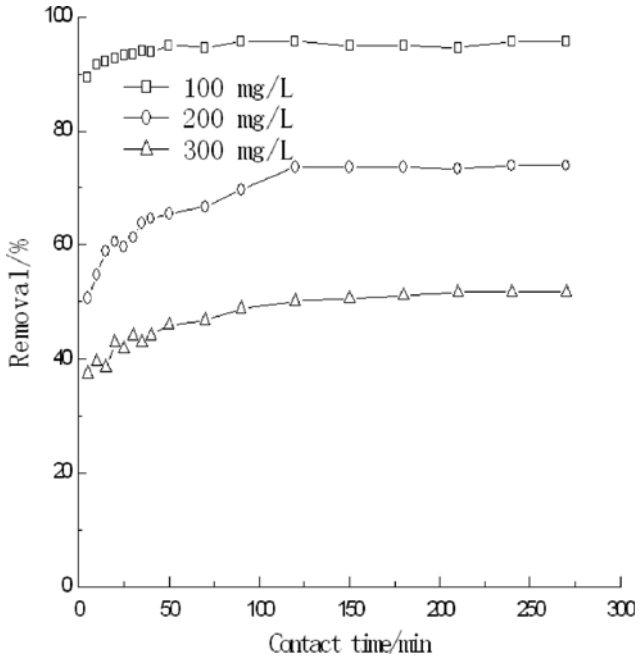

Fig. 7. Effect of contact time on Cr(VI) adsorption.

6. Adsorption Kinetics

To elucidate the adsorption process of Cr(IV) on CCB, several commonly used adsorption kinetic models were employed to discuss the controlling mechanism. Several kinetic models such as pseudo-first-order, pseudo-second-order, intraparticle diffusion and film-diffusion model have been applied to find the adsorption mechanism. Table 2 shows the results of the kinetic parameters for adsorption of Cr(VI) ions onto CCB.

The pseudo-first-order model of Lagergren is based on the assumption that the rate of change of adsorbed solute with time is proportional to the difference in equilibrium adsorption capacity and the adsorbed amount [28]:

$$\frac{1}{q_t} = \frac{k_1}{q_e t} + \frac{1}{q_e} \quad (3)$$

where q_e and q_t are the amounts of adsorbate adsorbed (mg/g) at equilibrium and at contact time t (min), respectively, and k_1 is the pseudo-first-order rate constant (min^{-1}). The straight-line plots of $1/q_t$ versus 1/t (Fig. 8(a)) were used to determine the values of k_1, q_e, and correlation coefficients (R^2). Although the calculated q_e values almost agreed with the experimental ones, the values of R^2 for the pseudo-first-order kinetic model were relatively low (Table 2). This indicates that the pseudo-first-order kinetic model cannot

Table 2. Kinetic parameters for adsorption of Cr(VI) ions onto cross-linked chitosan/bentonite composite

C_0/ mg/L	$q_{e,exp}$/ mg/g	Pseudo-first order model			Pseudo-second order model			Elovich model			Intraparticle diffusion model		
		R^2	k_1/ min^{-1}	$q_{e,cal}$/ mg/g	R^2	k_2/g/ mg/min	$q_{e,cal}$/ mg/g	R^2	β/ g/mg	α/mg/ g/min	R^2	K_p/mg/ $g/min^{0.5}$	C
100	47.85	0.9415	0.4950	47.73	0.9998	0.0542	47.69	0.9845	0.9748	1.245E+14	0.9375	2.620	44.51
200	73.95	0.9371	3.859	72.52	0.9998	0.0023	75.59	0.9871	0.1615	4.758E+03	0.9380	0.654	52.76
300	77.45	0.9043	3.710	75.64	0.9999	0.0021	79.11	0.9822	0.1646	9.379E+03	0.9560	0.651	55.69

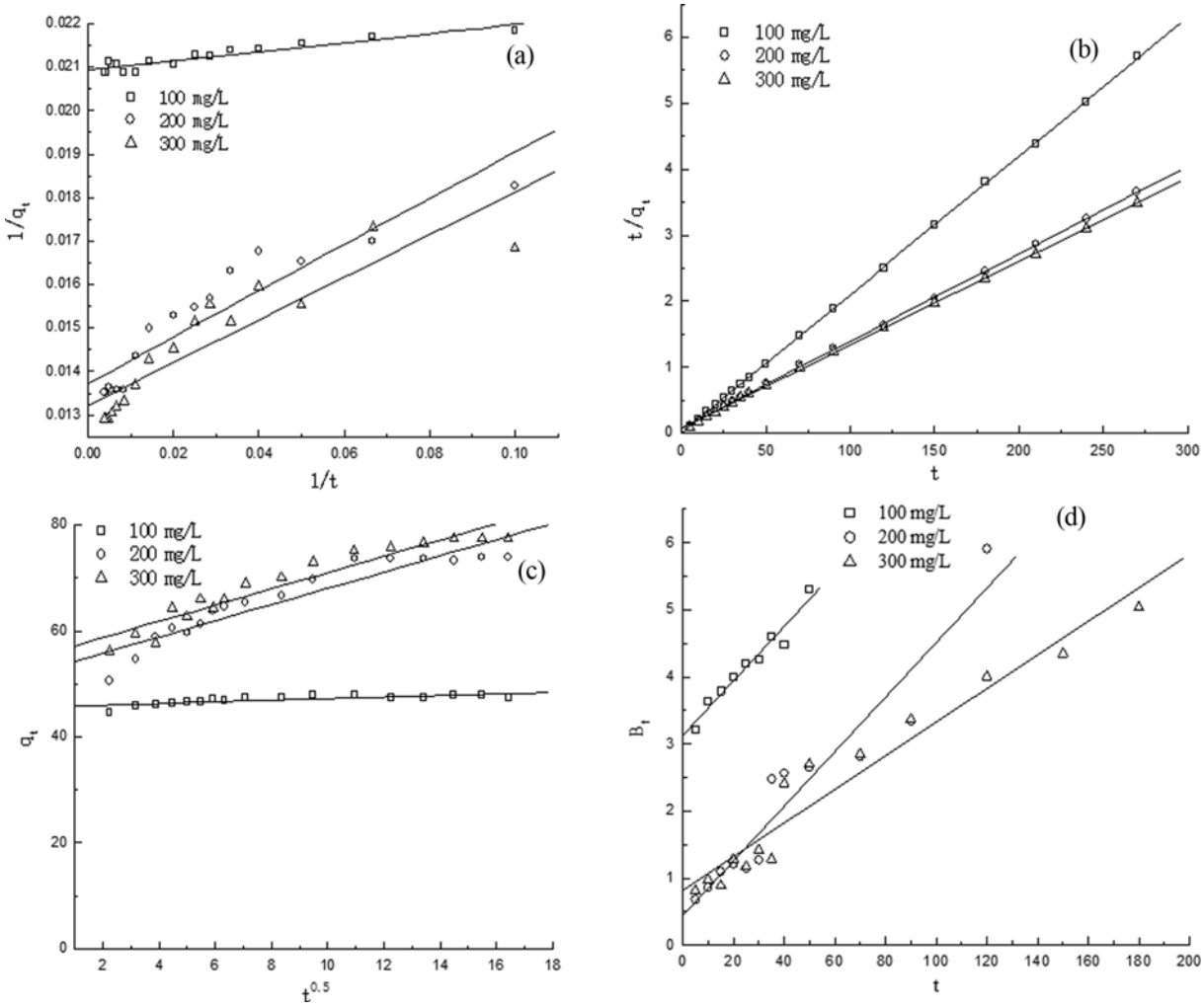

Fig. 8. Adsorption kinetic models of Cr(VI) ions by cross-linked chitosan/bentonite composite: (a) pseudo-first-order kinetic model; (b) pseudo-second-order kinetic model; (c) intraparticle diffusion model; (d) film-diffusion model.

describe adequately the adsorption of Cr(IV) on CCB.

The pseudo-second-order model is based on the assumption that the rate-limiting step involves chemisorption [29]. The linear form of the pseudo-second-order kinetic model is expressed as follows:

$$\frac{t}{q_t} = \frac{1}{k_2 q_e^2} + \frac{1}{q_e} t \quad (4)$$

where k_2 is the rate constant of pseudo-second-order adsorption (g/(mg·min)). The straight-line plots of t/q_t versus t (Fig. 8(b)) were used to determine the values of k_2, q_e and correlation coefficient (R^2). The linear plots of t/q_t versus t show a good agreement with the experimental data due to high values of R^2 (close to 1). Furthermore, the calculated q_e values agreed very well with the experimental ones at all initial Cr(IV) ions concentrations (Table 2). The adsorption of Cr(IV) on CCB obeyed the pseudo-second-order kinetic model for the whole adsorption period. This phenomenon suggests that the rate-limiting step might be chemisorption involving the chemical action between adsorbent and adsorbate. Besides, the values of k_2 for the adsorption of Cr(IV) on CCB were found to decrease from 0.0542 to 0.0021 g/(mg·min) with an increase in concentrations from 100 to 300 mg/L, suggesting that the contact time required for equilibrium at high concentration was relatively longer, as shown in Fig. 7.

The intraparticle diffusion model is used to investigate the diffusion controlled adsorption system. The intraparticle diffusion was explored by using Eq. (5):

$$q_t = k_p t^{0.5} + C \quad (5)$$

where k_p is the intraparticle diffusion rate constant (mg/(g·min$^{0.5}$)) and C is the slope that represents the thickness of the boundary layer: the larger the intercept, the greater is the boundary effect. The plots of q_t vs. the square root of time obtained for the adsorption of Cr(IV) onto CCB at different concentrations are shown in Fig. 8(c). They were not linear over the whole time range, indicating that more than one step was involved in the adsorption of Cr(IV) ions. If the intraparticle diffusion is the only rate-controlling step, then the plot should pass through the origin, else the boundary layer diffusion affects the adsorption to some degree. These plots were not passing through origin, indicating that the intraparticle diffusion was not the only rate determining factor during the grad-

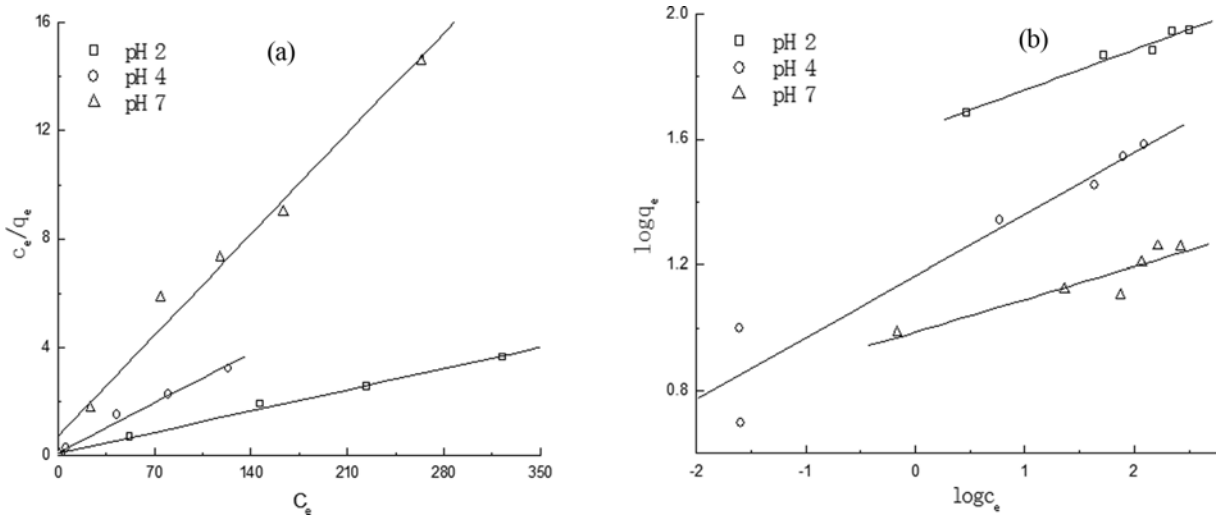

Fig. 9. Adsorption isotherm models of Cr(VI) by cross-linked chitosan/bentonite composite: (a) Langmuir model; (b) Freundlich model.

ual adsorption stage, and external mass transfer (boundary layer diffusion) and intraparticle diffusion took place simultaneously during the gradual adsorption stage.

The film-diffusion model of Boyd is a single-resistance model that assumes the main resistance to diffusion is in the boundary layer surrounding the adsorbent particle and is expressed as:

$$F=1-\frac{6}{\pi^2}\sum_{n=1}^{\infty}\frac{1}{n^2}\exp(-n^2B_t) \quad (6)$$

where, F is the fractional attainment of equilibrium, at different times, t, and expressed as

$$F=\frac{q_t}{q_e} \quad (7)$$

For F>0.85,

$$B_t=-0.4977-\ln(1-F) \quad (8)$$

and for F<0.85,

$$B_t=\left(\sqrt{\pi}-\sqrt{\pi-\left(\frac{\pi^2F}{3}\right)}\right)^2 \quad (9)$$

where q_t (mg/g) is the amount of solute adsorbed at time t, q_e (mg/g) is the maximum amount of arsenate adsorbed at equilibrium, B_t is the mathematical function of F, n is an integer that defines the infinite series solution. The B_t values calculated from the above equations are plotted against time t (Fig. 8(d)). The linear lines for all Cr(IV) initial concentrations did no pass through the origin and the points were scattered. This indicated that the adsorption of Cr(IV) on the CCB composite was mainly governed by external mass transport where particle diffusion was the rate limiting step. This is in accordance with the result obtained from the intraparticle diffusion model [30,31].

7. Adsorption Equilibrium

The isotherm study was carried out at various pH values (2, 4 and 7). Isotherm models, namely Langmuir model and Freundlich model, were used to describe the interaction between the solute and the adsorbent. The Langmuir isotherm describes an adsorption occurring on the surface that has a finite number of sites with similar energy levels. It is a model based on the following assumptions: homogeneous adsorption occurring on a monolayer surface coverage and without net interaction between the adsorbed species [32]. The Langmuir isotherm can be represented as Eq. (10):

$$\frac{C_e}{q_e}=\frac{1}{Qb}+\frac{C_e}{Q} \quad (10)$$

where C_e is the concentration of Cr(IV) ions at equilibrium (mg/L), q_e is the amount of Cr(IV) ions adsorbed per unit of adsorbent at equilibrium (mg/g), Q is the maximum amount of adsorption with complete monolayer coverage on the adsorbent surface (mg/g), and b is the Langmuir constant, which is related to the energy of adsorption (L/mg). Langmuir constants can be estimated from the linear plot of C_e/q_e versus C_e.

The Freundlich model assumes a heterogeneous surface with the involvement of sites of different energies in the adsorption process [33]. The Freundlich isotherm can be represented as Eq. (11):

$$\log q_e=\log k_f+\frac{1}{n}\log C_e \quad (11)$$

where q_e is the amount of Cr(IV) ions adsorbed per unit of adsorbent at equilibrium (mg/g), C_e is the concentration of Cr(IV) ions at equilibrium (mg/L), k_f ((mg/g)(L/mg)$^{1/n}$), and n are Freundlich

Table 3. Isotherm parameters for Cr(VI) ions adsorption by cross-linked chitosan/bentonite composite

Isotherm models	pH 2	pH 4	pH 7
Langmuir			
Q	89.13	37.92	18.78
b	0.1380	0.2469	0.0746
R^2	0.9977	0.9933	0.9918
Freundlich			
K_f	42.65	14.64	9.72
n	7.800	5.097	9.662
R^2	0.9878	0.9598	0.9232

Table 4. Comparison of the maximum monolayer adsorption capacities of Cr(VI) on various adsorbents

Adsorbent	pH	Adsorption capacity/mg/g	References
Oak wood charcoal	2	30.10	[34]
Oak wood charcoal ash	2.5	46.17	[34]
Amino-functionalized magnetic cellulose composite	2.0	171.5	[35]
Mesoporous NiO nanoparticles	4.7	4.73	[36]
KIP210 resin	3	100	[37]
Ammonium sulfamate-bacterial cellulose	1.5	22.73	[38]
Tannin-immobilized activated clay	2.5	24.09	[39]
Cross-linked chitosan/bentonite composite	2	89.13	This study

constants related to adsorption capacity and heterogeneity factor, respectively. The values of k_f and n can be obtained from the slope and intercept of the plot of $\log q_e$ versus $\log C_e$.

The linearized Langmuir and Freundlich isotherms for the adsorption of Cr(IV) on CCB are shown in Fig. 9. The fitting parameters for Cr(IV) adsorption isotherms based on Langmuir and Freundlich equations are listed in Table 3. The fitting results show that the correlation coefficient values of Langmuir isotherm model were higher than those of the Freundlich isotherm model, indicating that the adsorption of Cr(IV) on CCB can be correlated by the Langmuir isotherm model. The adsorption of Cr(IV) on CCB was attributed to a monolayer adsorption. The maximum monolayer Cr(IV) adsorption capacity for CCB at pH 2 and 293 K was found to be 89.13 mg/g. The maximum adsorption capacity decreased with an increase in pH value. A comparison of Cr(IV) adsorption capacity of CCB with previously employed adsorbents is given in Table 4. It is evident that CCB had a relatively high adsorption capacity for Cr(IV) ions. High adsorption capacity indicates that CCB would be a promising adsorbent in the removal of Cr(IV) ions from aqueous solutions.

CONCLUSION

Cross-linked chitosan/bentonite composite (CCB) was prepared, and characterized by FTIR spectroscopy and XRD patterns. The XRD results of CCB show that cross-linked chitosan intercalated into bentonite. FTIR analyses showed the amino groups in CCB were the main adsorption sites of Cr(IV) ions. The removal towards Cr(IV) ions decreased with increasing solution pH from 2 to 11 and initial Cr(IV) ions concentrations, while it increased with increasing adsorbent dosage. The adsorption kinetics of Cr(IV) on CCB obeyed the pseudo-second-order model. Intraparticle diffusion is not the only rate-controlling step. The equilibrium adsorption data of Cr(IV) ions onto CCB were described by the Langmuir isotherm model. The maximum monolayer Cr(IV) adsorption capacity on CCB at pH 2 and 293 K was 89.13 mg/g. The mechanisms for the adsorption of Cr(IV) adsorption onto CCB at pH 2 may include electrostatic interaction and chemical interaction between CCB and Cr(IV).

ACKNOWLEDGEMENT

This work was supported by the National Natural Science Foundation of China (Grant No. 51003086).

REFERENCES

1. E. Margarita, R. Carmona, P. Moñica A, da Silva, G. Selma and F. Leite, *J. Taiwan Inst. Chem. Eng.*, **43**, 428 (2012).
2. J. Li, S. Chen, G. Sheng, J. Hu, X. Tan and X. Wang. *Chem. Eng. J.*, **166**, 551 (2011).
3. Q. Wang, J. Li, C. Chen, X. Ren, J. Hu and X. Wang, *Chem. Eng. J.*, **174**, 126 (2011).
4. J. Li, J. Hu, G. Sheng, G. Zhao and Q. Huang, *Colloids Surf., A.*, **349**, 195 (2009).
5. D. Saravanana, T. Gomathib and P. N. Sudhab, *Int. J. Biol. Macrom.*, **53**, 67 (2013).
6. C. Shen, H. Chen, S. Wu, Y. Wen, L. Li, Z. Jiang, M. Li and W. Liu, *J. Hazard. Mater.*, **244-245**, 689 (2013).
7. W. S. Wan Ngah, L. C. Teong and M. A. K. M. Hanafiah, *Carbohyd. Polym.*, **83**, 1446 (2011).
8. P. Miretzky and A. F. Cirelli, *J. Fluorine. Chem.*, **132**, 231 (2011).
9. W. S. Wan Ngah, S. Fatinathan and N. A. Yosop, *Desalination*, **293**, 272 (2011).
10. Y. H. Deng, L. Wang, X. B. Hu, B. Z. Liu, Z. B. Wei, S. G. Yang and C. Sun, *Chem. Eng. J.*, **181-182**, 300 (2012).
11. X. H. Zou, J. M. Pan, H. X. Ou, X. Wang, W. Guan, C. X. Li, Y. S. Yan and Y. Q. Duan, *Chem. Eng. J.*, **167**, 112 (2011).
12. C. M. Futalan, C. C. Kan, M. L. Dalida, K. J. Hsien, C. Pascua and M. W. Wan, *Carbohyd. Polym.*, **83**, 528 (2011).
13. M. L. P. Dalida, A. F. V. Mariano, C. M. Futalan, C. C. Kan, W. C. Tsai and M. W. Wan, *Desalination*, **275**, 154 (2011).
14. D. Chen, W. Li, Y. Wu, Q. Zhu, Z. Lu and G. Du, *Chem. Eng. J.*, **221**, 8 (2013).
15. F. A. R. Pereira, K. S. Sousa, G. R. S. Cavalcanti, M. G. Fonseca, A. G. deSouza and A. P. M. Alves, *Int. J. Biol. Macromol.*, **61**, 471 (2013).
16. M. Y. Chang and R. S. J. Juang, *Colloid Interface Sci.*, **278**, 18 (2004).
17. C. Muzzarelli, O. Francescanheli, G. Tosi and R. A. A. Muzzarelli, *Carbohyd. Polym.*, **56**, 137 (2004).
18. W. Tan, Y. Zhang, Y. S. Szeto and L. Liao, *Compos. Sci. Technol.*, **68**, 2917 (2008).
19. P. Monvisade and P. Siriphannon, *Appl. Clay Sci.*, **42**, 427 (2009).
20. C. Paluszkiewicz, E. Stodolak, M. Hasik and M. Blazewicz, *Spectrochim. Acta A. Mol. Biomol. Spectrosc.*, **79**, 784 (2011).
21. A. R. Nesic, S. J. Velickovic and D. G. Antonovic, *J. Hazard. Mater.*,

256, 209 (2012).
22. Z. Li, W. T. Jiang and H. Hong, *Spectrochim. Acta A. Mol. Biomol. Spectrosc.*, **71**, 1525 (2008).
23. W. A. Zhang, D. Z. Chen, H. Y. Xu, X. F. Shen and Y. E. Fang, *Eur. Polym. J.*, **39**, 2323 (2003).
24. R. Ansari and N. Khoshbakht Fahim, *React. Funct. Polym.*, **67**, 367 (2007).
25. H. Javadian, M. Ahmadi, M. Ghiasvand, S. Kahrizi and R. Katal, *J. Taiwan Inst. Chem. E.*, **44**, 977 (2013).
26. H. Uslu, *Chem. Eng. J.*, **155**, 320 (2009).
27. S. Gupta and B. V. Babu, *Chem. Eng. J.*, **150**, 352 (2009).
28. X. Han, W. Wang and X. Ma. *Chem. Eng. J.*, **171**, 1 (2011).
29. Q. Qin, J. Ma and K. Liu, *J. Hazard. Mater.*, **162**, 133 (2009).
30. B. H. Hameed, I. A. W. Tan and A. L. Ahmad, *Chem. Eng. J.*, **144**, 235 (2008).
31. P. Sharma and M. R. Das, *J. Chem. Eng. Data*, **58**, 151 (2013).
32. S. Gao, R. Sun, Z. G. Wei, H. Y. Zhao and H. X. Li, *J. Fluorine Chem.*, **130**(6), 550 (2009).
33. N. Barka, A. Assabbane, A. Nounah, L. Laanab and Y. A. Ichou, *Desalination*, **235**(1), 264 (2009).
34. E. Pehlivan, H. Kahraman and E. Pehlivan, *Fuel Process. Technol.*, **92**, 65 (2011).
35. X. Sun, L. Yang, Q. Li, J. Zhao, X. Li, X. Wang and H. Liu, *Chem. Eng. J.*, **241**, 175 (2014).
36. M. A. Behnajady and S. Bimeghdar, *Chem. Eng. J.*, **239**, 105 (2014).
37. J. Yang, M. Yu and T. Qiu, *J. Ind. Eng. Chem.*, **20**, 480 (2014).
38. M. Lu, X. Guan, X. Xu and D. Wei, *Chinese. Chem. Lett.*, **24**, 253 (2013).
39. W. Li, Y. Tang, Z. Tong, D. Liang and W. Cui, *Chem. Eng. J.*, **193-194**, 88 (2012).